# Study of J/ψ→pp[over ¯]φ at BESIII

M. Ablikim *et al.* (BESIII Collaboration)

# Study of $J/\psi \to p\bar{p}\phi$ at BESIII

M. Ablikim[1], M. N. Achasov[9,e], X. C. Ai[1], O. Albayrak[5], M. Albrecht[4], D. J. Ambrose[44], A. Amoroso[49A,49C], F. F. An[1], Q. An[46,a], J. Z. Bai[1], R. Baldini Ferroli[20A], Y. Ban[31], D. W. Bennett[19], J. V. Bennett[5], M. Bertani[20A], D. Bettoni[21A], J. M. Bian[43], F. Bianchi[49A,49C], E. Boger[23,c], I. Boyko[23], R. A. Briere[5], H. Cai[51], X. Cai[1,a], O. Cakir[40A], A. Calcaterra[20A], G. F. Cao[1], S. A. Cetin[40B], J. F. Chang[1,a], G. Chelkov[23,c,d], G. Chen[1], H. S. Chen[1], H. Y. Chen[2], J. C. Chen[1], M. L. Chen[1,a], S. J. Chen[29], X. Chen[1,a], X. R. Chen[26], Y. B. Chen[1,a], H. P. Cheng[17], X. K. Chu[31], G. Cibinetto[21A], H. L. Dai[1,a], J. P. Dai[34], A. Dbeyssi[14], D. Dedovich[23], Z. Y. Deng[1], A. Denig[22], I. Denysenko[23], M. Destefanis[49A,49C], F. De Mori[49A,49C], Y. Ding[27], C. Dong[30], J. Dong[1,a], L. Y. Dong[1], M. Y. Dong[1,a], Z. L. Dou[29], S. X. Du[53], P. F. Duan[1], J. Z. Fan[39], J. Fang[1,a], S. S. Fang[1], X. Fang[46,a], Y. Fang[1], R. Farinelli[21A,21B], L. Fava[49B,49C], O. Fedorov[23], F. Feldbauer[22], G. Felici[20A], C. Q. Feng[46,a], E. Fioravanti[21A], M. Fritsch[14,22], C. D. Fu[1], Q. Gao[1], X. L. Gao[46,a], X. Y. Gao[2], Y. Gao[39], Z. Gao[46,a], I. Garzia[21A], K. Goetzen[10], L. Gong[30], W. X. Gong[1,a], W. Gradl[22], M. Greco[49A,49C], M. H. Gu[1,a], Y. T. Gu[12], Y. H. Guan[1], A. Q. Guo[1], L. B. Guo[28], Y. Guo[1], Y. P. Guo[22], Z. Haddadi[25], A. Hafner[22], S. Han[51], X. Q. Hao[15], F. A. Harris[42], K. L. He[1], T. Held[4], Y. K. Heng[1,a], Z. L. Hou[1], C. Hu[28], H. M. Hu[1], J. F. Hu[49A,49C], T. Hu[1,a], Y. Hu[1], G. S. Huang[46,a], J. S. Huang[15], X. T. Huang[33], Y. Huang[29], T. Hussain[48], Q. Ji[1], Q. P. Ji[30], X. B. Ji[1], X. L. Ji[1,a], L. W. Jiang[51], X. S. Jiang[1,a], X. Y. Jiang[30], J. B. Jiao[33], Z. Jiao[17], D. P. Jin[1,a], S. Jin[1], T. Johansson[50], A. Julin[43], N. Kalantar-Nayestanaki[25], X. L. Kang[1], X. S. Kang[30], M. Kavatsyuk[25], B. C. Ke[5], P. Kiese[22], R. Kliemt[14], B. Kloss[22], O. B. Kolcu[40B,h], B. Kopf[4], M. Kornicer[42], W. Kühn[24], A. Kupsc[50], J. S. Lange[24,a], M. Lara[19], P. Larin[14], C. Leng[49C], C. Li[50], Cheng Li[46,a], D. M. Li[53], F. Li[1,a], F. Y. Li[31], G. Li[1], H. B. Li[1], J. C. Li[1], Jin Li[32], K. Li[13], K. Li[33], Lei Li[3], P. R. Li[41], Q. Y. Li[33], T. Li[33], W. D. Li[1], W. G. Li[1], X. L. Li[33], X. M. Li[12], X. N. Li[1,a], X. Q. Li[30], Z. B. Li[38], H. Liang[46,a], Y. F. Liang[36], Y. T. Liang[24], G. R. Liao[11], D. X. Lin[14], B. J. Liu[1], C. X. Liu[1], D. Liu[46,a], F. H. Liu[35], Fang Liu[1], Feng Liu[6], H. B. Liu[12], H. H. Liu[1], H. H. Liu[16], H. M. Liu[1], J. Liu[1], J. B. Liu[46,a], J. P. Liu[51], J. Y. Liu[1], K. Liu[39], K. Y. Liu[27], L. D. Liu[31], P. L. Liu[1,a], Q. Liu[41], S. B. Liu[46,a], X. Liu[26], Y. B. Liu[30], Z. A. Liu[1,a], Zhiqing Liu[22], H. Loehner[25], X. C. Lou[1,a,g], H. J. Lu[17], J. G. Lu[1,a], Y. Lu[1], Y. P. Lu[1,a], C. L. Luo[28], M. X. Luo[52], T. Luo[42], X. L. Luo[1,a], X. R. Lyu[41], F. C. Ma[27], H. L. Ma[1], L. L. Ma[33], Q. M. Ma[1], T. Ma[1], X. N. Ma[30], X. Y. Ma[1,a], Y. M. Ma[33], F. E. Maas[14], M. Maggiora[49A,49C], Y. J. Mao[31], Z. P. Mao[1], S. Marcello[49A,49C], J. G. Messchendorp[25], J. Min[1,a], R. E. Mitchell[19], X. H. Mo[1,a], Y. J. Mo[6], C. Morales Morales[14], N. Yu. Muchnoi[9,e], H. Muramatsu[43], Y. Nefedov[23], F. Nerling[14], I. B. Nikolaev[9,e], Z. Ning[1,a], S. Nisar[8], S. L. Niu[1,a], X. Y. Niu[1], S. L. Olsen[32], Q. Ouyang[1,a], S. Pacetti[20B], Y. Pan[46,a], P. Patteri[20A], M. Pelizaeus[4], H. P. Peng[46,a], K. Peters[10], J. Pettersson[50], J. L. Ping[28], R. G. Ping[1], R. Poling[43], V. Prasad[1], H. R. Qi[2], M. Qi[29], S. Qian[1,a], C. F. Qiao[41], L. Q. Qin[33], N. Qin[51], X. S. Qin[1], Z. H. Qin[1,a], J. F. Qiu[1], K. H. Rashid[48], C. F. Redmer[22], M. Ripka[22], G. Rong[1], Ch. Rosner[14], X. D. Ruan[12], V. Santoro[21A], A. Sarantsev[23,f], M. Savrié[21B], K. Schoenning[50], S. Schumann[22], W. Shan[31], M. Shao[46,a], C. P. Shen[2], P. X. Shen[30], X. Y. Shen[1], H. Y. Sheng[1], W. M. Song[1], X. Y. Song[1], S. Sosio[49A,49C], S. Spataro[49A,49C], G. X. Sun[1], J. F. Sun[15], S. S. Sun[1], Y. J. Sun[46,a], Y. Z. Sun[1], Z. J. Sun[1,a], Z. T. Sun[19], C. J. Tang[36], X. Tang[1], I. Tapan[40C], E. H. Thorndike[44], M. Tiemens[25], M. Ullrich[24], I. Uman[40D], G. S. Varner[42], B. Wang[30], B. L. Wang[41], D. Wang[31], D. Y. Wang[31], K. Wang[1,a], L. L. Wang[1], L. S. Wang[1], M. Wang[33], P. Wang[1], P. L. Wang[1], S. G. Wang[31], W. Wang[1,a], W. P. Wang[46,a], X. F. Wang[39], Y. D. Wang[14], Y. F. Wang[1,a], Y. Q. Wang[22], Z. Wang[1,a], Z. G. Wang[1,a], Z. H. Wang[46,a], Z. Y. Wang[1], T. Weber[22], D. H. Wei[11], J. B. Wei[31], P. Weidenkaff[22], S. P. Wen[1], U. Wiedner[4], M. Wolke[50], L. H. Wu[1], Z. Wu[1,a], L. Xia[46,a], L. G. Xia[39], Y. Xia[18], D. Xiao[1], H. Xiao[47], Z. J. Xiao[28], Y. G. Xie[1,a], Q. L. Xiu[1,a], G. F. Xu[1], L. Xu[1], Q. J. Xu[13], Q. N. Xu[41], X. P. Xu[37], L. Yan[49A,49C], W. B. Yan[46,a], W. C. Yan[46,a], Y. H. Yan[18], H. J. Yang[34], H. X. Yang[1], L. Yang[51], Y. X. Yang[11], M. Ye[1,a], M. H. Ye[7], J. H. Yin[1], B. X. Yu[1,a], C. X. Yu[30], J. S. Yu[26], C. Z. Yuan[1], W. L. Yuan[29], Y. Yuan[1], A. Yuncu[40B,b], A. A. Zafar[48], A. Zallo[20A], Y. Zeng[18], Z. Zeng[46,a], B. X. Zhang[1], B. Y. Zhang[1,a], C. Zhang[29], C. C. Zhang[1], D. H. Zhang[1], H. H. Zhang[38], H. Y. Zhang[1,a], J. J. Zhang[1], J. L. Zhang[1], J. Q. Zhang[1], J. W. Zhang[1,a], J. Y. Zhang[1], J. Z. Zhang[1], K. Zhang[1], L. Zhang[1], X. Y. Zhang[33], Y. Zhang[1], Y. H. Zhang[1,a], Y. N. Zhang[41], Y. T. Zhang[46,a], Yu Zhang[41], Z. H. Zhang[6], Z. P. Zhang[46], Z. Y. Zhang[51], G. Zhao[1], J. W. Zhao[1,a], J. Y. Zhao[1], J. Z. Zhao[1,a], Lei Zhao[46,a], Ling Zhao[1], M. G. Zhao[30], Q. Zhao[1], Q. W. Zhao[1], S. J. Zhao[53], T. C. Zhao[1], Y. B. Zhao[1,a], Z. G. Zhao[46,a], A. Zhemchugov[23,c], B. Zheng[47], J. P. Zheng[1,a], W. J. Zheng[33], Y. H. Zheng[41], B. Zhong[28], L. Zhou[1,a], X. Zhou[51], X. K. Zhou[46,a], X. R. Zhou[46,a], X. Y. Zhou[1], K. Zhu[1], K. J. Zhu[1,a], S. Zhu[1], S. H. Zhu[45], X. L. Zhu[39], Y. C. Zhu[46,a], Y. S. Zhu[1], Z. A. Zhu[1], J. Zhuang[1,a], L. Zotti[49A,49C], B. S. Zou[1], J. H. Zou[1]

(BESIII Collaboration)

[1] *Institute of High Energy Physics, Beijing 100049, People's Republic of China*
[2] *Beihang University, Beijing 100191, People's Republic of China*
[3] *Beijing Institute of Petrochemical Technology, Beijing 102617, People's Republic of China*
[4] *Bochum Ruhr-University, D-44780 Bochum, Germany*
[5] *Carnegie Mellon University, Pittsburgh, Pennsylvania 15213, USA*
[6] *Central China Normal University, Wuhan 430079, People's Republic of China*
[7] *China Center of Advanced Science and Technology, Beijing 100190, People's Republic of China*
[8] *COMSATS Institute of Information Technology, Lahore, Defence Road, Off Raiwind Road, 54000 Lahore, Pakistan*
[9] *G.I. Budker Institute of Nuclear Physics SB RAS (BINP), Novosibirsk 630090, Russia*
[10] *GSI Helmholtzcentre for Heavy Ion Research GmbH, D-64291 Darmstadt, Germany*
[11] *Guangxi Normal University, Guilin 541004, People's Republic of China*
[12] *GuangXi University, Nanning 530004, People's Republic of China*

[13] *Hangzhou Normal University, Hangzhou 310036, People's Republic of China*

[14] *Helmholtz Institute Mainz, Johann-Joachim-Becher-Weg 45, D-55099 Mainz, Germany*

[15] *Henan Normal University, Xinxiang 453007, People's Republic of China*

[16] *Henan University of Science and Technology, Luoyang 471003, People's Republic of China*

[17] *Huangshan College, Huangshan 245000, People's Republic of China*

[18] *Hunan University, Changsha 410082, People's Republic of China*

[19] *Indiana University, Bloomington, Indiana 47405, USA*

[20] *(A)INFN Laboratori Nazionali di Frascati, I-00044, Frascati, Italy; (B)INFN and University of Perugia, I-06100, Perugia, Italy*

[21] *(A)INFN Sezione di Ferrara, I-44122, Ferrara, Italy; (B)University of Ferrara, I-44122, Ferrara, Italy*

[22] *Johannes Gutenberg University of Mainz, Johann-Joachim-Becher-Weg 45, D-55099 Mainz, Germany*

[23] *Joint Institute for Nuclear Research, 141980 Dubna, Moscow region, Russia*

[24] *Justus Liebig University Giessen, II. Physikalisches Institut, Heinrich-Buff-Ring 16, D-35392 Giessen, Germany*

[25] *KVI-CART, University of Groningen, NL-9747 AA Groningen, The Netherlands*

[26] *Lanzhou University, Lanzhou 730000, People's Republic of China*

[27] *Liaoning University, Shenyang 110036, People's Republic of China*

[28] *Nanjing Normal University, Nanjing 210023, People's Republic of China*

[29] *Nanjing University, Nanjing 210093, People's Republic of China*

[30] *Nankai University, Tianjin 300071, People's Republic of China*

[31] *Peking University, Beijing 100871, People's Republic of China*

[32] *Seoul National University, Seoul, 151-747 Korea*

[33] *Shandong University, Jinan 250100, People's Republic of China*

[34] *Shanghai Jiao Tong University, Shanghai 200240, People's Republic of China*

[35] *Shanxi University, Taiyuan 030006, People's Republic of China*

[36] *Sichuan University, Chengdu 610064, People's Republic of China*

[37] *Soochow University, Suzhou 215006, People's Republic of China*

[38] *Sun Yat-Sen University, Guangzhou 510275, People's Republic of China*

[39] *Tsinghua University, Beijing 100084, People's Republic of China*

[40] *(A)Ankara University, 06100 Tandogan, Ankara, Turkey; (B)Istanbul Bilgi University, 34060 Eyup, Istanbul, Turkey; (C)Uludag University, 16059 Bursa, Turkey; (D)Near East University, Nicosia, North Cyprus, Mersin 10, Turkey*

[41] *University of Chinese Academy of Sciences, Beijing 100049, People's Republic of China*

[42] *University of Hawaii, Honolulu, Hawaii 96822, USA*

[43] *University of Minnesota, Minneapolis, Minnesota 55455, USA*

[44] *University of Rochester, Rochester, New York 14627, USA*

[45] *University of Science and Technology Liaoning, Anshan 114051, People's Republic of China*

[46] *University of Science and Technology of China, Hefei 230026, People's Republic of China*

[47] *University of South China, Hengyang 421001, People's Republic of China*

[48] *University of the Punjab, Lahore-54590, Pakistan*

[49] *(A)University of Turin, I-10125, Turin, Italy; (B)University of Eastern Piedmont, I-15121, Alessandria, Italy; (C)INFN, I-10125, Turin, Italy*

[50] *Uppsala University, Box 516, SE-75120 Uppsala, Sweden*

[51] *Wuhan University, Wuhan 430072, People's Republic of China*

[52] *Zhejiang University, Hangzhou 310027, People's Republic of China*

[53] *Zhengzhou University, Zhengzhou 450001, People's Republic of China*

[a] *Also at State Key Laboratory of Particle Detection and Electronics, Beijing 100049, Hefei 230026, People's Republic of China*

[b] *Also at Bogazici University, 34342 Istanbul, Turkey*

[c] *Also at the Moscow Institute of Physics and Technology, Moscow 141700, Russia*

[d] *Also at the Functional Electronics Laboratory, Tomsk State University, Tomsk, 634050, Russia*

[e] *Also at the Novosibirsk State University, Novosibirsk, 630090, Russia*

[f] *Also at the NRC "Kurchatov Institute", PNPI, 188300, Gatchina, Russia*

[g] *Also at University of Texas at Dallas, Richardson, Texas 75083, USA*

[h] *Also at Istanbul Arel University, 34295 Istanbul, Turkey*

Using a data sample of $1.31 \times 10^9$ $J/\psi$ events accumulated with the BESIII detector, the decay $J/\psi \to p\bar{p}\phi$ is studied via two decay modes, $\phi \to K_S^0 K_L^0$ and $\phi \to K^+ K^-$. The branching fraction of $J/\psi \to p\bar{p}\phi$ is measured to be $\mathcal{B}(J/\psi \to p\bar{p}\phi) = [5.23 \pm 0.06\,(\text{stat}) \pm 0.33\,(\text{syst})] \times 10^{-5}$, which agrees well with a previously published measurement, but with a significantly improved precision. No evident enhancement near the $p\bar{p}$ mass threshold, denoted as $X(p\bar{p})$, is observed, and the upper limit on the branching fraction of $J/\psi \to X(p\bar{p})\phi \to p\bar{p}\phi$ is determined to be $\mathcal{B}(J/\psi \to X(p\bar{p})\phi \to p\bar{p}\phi) < 2.1 \times 10^{-7}$ at the 90% confidence level.

## I. INTRODUCTION

In 2003, a strong enhancement near the $p\bar{p}$ mass threshold, known as the $X(p\bar{p})$, was first observed by the BESII experiment in the radiative decay $J/\psi \to \gamma p\bar{p}$ [1]. It was later confirmed by the CLEO and BESIII experiments [2–4]. Strikingly, no corresponding enhancements were observed either in $\Upsilon(1S) \to \gamma p\bar{p}$ [5] radiative decays or in hadronic decays of vector charmonium states below the open-charm threshold, e.g. $J/\psi(\psi(3686)) \to \pi^0 p\bar{p}$ [1, 6] and $J/\psi \to \omega p\bar{p}$ [7, 8].

The experimental observations of the $X(p\bar{p})$ structure in $J/\psi \to \gamma p\bar{p}$ and the absence in other probes raised many discussions in the community resulting in various speculations on its nature. The most popular theoretical interpretations include baryonium [9–11], a multiquark state [12] or an effect mainly due to pure final-state interaction (FSI) [13–16]. In accordance with the latest results of a partial wave analysis (PWA) [4], it was proposed to associate this enhancement with a new resonance, $X(1835)$, that was observed in the $J/\psi \to \gamma\pi^+\pi^-\eta'$ decay [17, 18]. The nature of the $X(p\bar{p})$ is still mysterious to date, therefore its investigation via other $J/\psi$ decay modes may shed light on its nature. The decay $J/\psi \to p\bar{p}\phi$ restricts the isospin of the $p\bar{p}$ system and is helpful to clarify the role of the $p\bar{p}$ FSI.

In this paper, we report on a search for a near-threshold enhancement in the $p\bar{p}$ mass spectrum and the possible $p\phi$ ($\bar{p}\phi$) resonances in the process $J/\psi \to p\bar{p}\phi$. The decay $J/\psi \to p\bar{p}\phi$ was investigated by the DM2 Collaboration based on $(8.6 \pm 1.3) \times 10^6$ $J/\psi$ events about thirty years ago [19], with a large uncertainty due to the limited statistics (only $17 \pm 5$ events were observed). In this work, the channel $J/\psi \to p\bar{p}\phi$ is studied via the two decay modes $\phi \to K_S^0 K_L^0$ and $\phi \to K^+ K^-$ using a data sample of $1.31 \times 10^9$ $J/\psi$ events [20, 21] accumulated with the BESIII detector.

## II. BESIII DETECTOR AND MONTE CARLO SIMULATION

The BESIII detector [22] is a general purpose spectrometer at the BEPCII $e^+e^-$ accelerator for studies of hadron spectroscopy as well as $\tau$-charm physics [23]. The BESIII detector with a geometrical acceptance of 93% of $4\pi$ consists of the following main components: 1) a small-cell, helium-based main drift chamber (MDC) with 43 layers, which measures tracks of charged particles and provides a measurement of the specific energy loss $dE/dx$. The average single wire resolution is 135 $\mu$m, and the momentum resolution for 1 GeV/$c$ charged particles in a 1 T magnetic field is 0.5%; 2) a Time-Of-Flight system (TOF) for particle identification (PID) composed of a barrel part constructed of two layers with 88 pieces of

5 cm thick, 2.4 m long plastic scintillators in each layer, and two end caps with 48 fan-shaped, 5 cm thick, plastic scintillators in each end cap. The time resolution is 80 ps (110 ps) in the barrel (end caps), corresponding to a $K/\pi$ separation of more than $2\sigma$ for momenta at 1 GeV/$c$ and below; 3) an electromagnetic calorimeter (EMC) consisting of 6240 CsI(Tl) crystals arranged in a cylindrical shape (barrel) plus two end caps. For 1 GeV/$c$ photons, the energy resolution is 2.5% (5%) in the barrel (end caps), and the position resolution is 6 mm (9 mm) in the barrel (end caps); 4) a muon chamber system (MUC) consists of about 1200 m$^2$ of Resistive Plate Chambers (RPC) arranged in 9 layers in the barrel and 8 layers in the end caps and incorporated in the return iron yoke of the superconducting magnet. The position resolution is about 2 cm.

The optimization of the event selection, the determination of the detector efficiency and the estimation of backgrounds are performed through Monte Carlo (MC) simulations. The GEANT4-based [24] simulation software BOOST [25] includes the geometric and material description of the BESIII detectors and models for the detector response and digitization, as well as the tracking of the detector running conditions and performance. For the background study, an inclusive MC sample of $1.23 \times 10^9$ $J/\psi$ decay events is generated. The production of the $J/\psi$ resonance is simulated by the MC event generator KKMC [26, 27], while the decays are generated by EVTGEN [28] for known decay modes with branching fractions being set to Particle Data Group (PDG) world average values [29], and by LUNDCHARM [30] for the remaining unknown decays. A sample of $2.0 \times 10^5$ events is generated for the three-body decay $J/\psi \to p\bar{p}\phi$ using a flat distribution in phase space (PHSP), and the signal detection efficiency is obtained by weighting the PHSP MC to data. For the decay $J/\psi \to X(p\bar{p})\phi \to p\bar{p}\phi$, a sample of $2.0 \times 10^5$ events is generated, and the angular distribution is considered in the simulation.

## III. EVENT SELECTION AND BACKGROUND ANALYSIS

Two dominant $\phi$ decays are used to reconstruct the $\phi$ meson in the study of the decay $J/\psi \to p\bar{p}\phi$, which allows us to check our measurements and to improve the precision of our results. In the following text, if not special specified, $K\bar{K}$ refers to both $K_S^0 K_L^0$ and $K^+ K^-$ final states.

### A. $J/\psi \to p\bar{p}\phi$, $\phi \to K_S^0 K_L^0$

In this decay channel, the $K_S^0$ is reconstructed in its decay to two charged pions, while the long-lived, diffi-

cult to detect, $K_L^0$ is taken as a missing particle. The event topology is therefore $p\bar{p}\pi^+\pi^-K_L^0$, and candidate events must have at least four charged tracks. Each of the charged track is reconstructed from MDC hits and the polar angle $\theta$ must satisfy $|\cos\theta| < 0.93$.

Two of the charged tracks are identified as proton and anti-proton by using combined TOF and $dE/dx$ information, while all other tracks are assumed to be charged pions without PID requirement. The identified proton and anti-proton are further required to originate from the same primary vertex and pass within 10 cm in the beam direction and within 1 cm in the radial direction with respect to the interaction point.

The $K_S^0$ meson is reconstructed by constraining a pair of oppositely charged pions to originate from a secondary vertex, and only candidate events with only one successfully reconstructed $K_S^0$ candidate are preserved for the further analysis. To suppress backgrounds, the chi-square of the second vertex fit is required to be less than 40. The scatter plot of the $\pi^+\pi^-$ invariant mass ($M_{\pi^+\pi^-}$) versus the recoiling mass against $p\bar{p}K_S^0$ ($M_{p\bar{p}K_S^0}^{\rm rec}$) is shown in Fig. 1, where a prominent $K_S^0 - K_L^0$ cluster corresponding to the signal channel of $J/\psi \to p\bar{p}K_S^0K_L^0$ is observed. Mass windows of $|M_{\pi^+\pi^-} - m_{K^0}| <5$ MeV/$c^2$ and $|M_{p\bar{p}K_S^0}^{\rm rec} - m_{K^0}| <15$ MeV/$c^2$ are required to identify signal events, where $m_{K^0}$ is the nominal mass of $K^0$ from PDG [29].
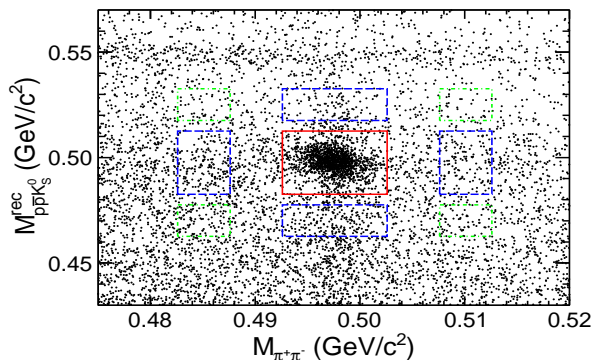


Figure 1. Scatter plot of the $\pi^+\pi^-$ invariant mass versus the recoiling mass against $p\bar{p}K_S^0$; the boxes represent the $K_S^0$ and $K_L^0$ signal region and sideband regions described in the text.

After applying the previously mentioned selection criteria, the recoil mass against the $p\bar{p}$ system, $M_{p\bar{p}}^{\rm rec}$, is examined, as shown in Fig. 2 (a), in which a clear $\phi$ signal is observed. To estimate the combinational backgrounds from non-$K_S^0$ or non-$K_L^0$ events, the background events in the $K_S^0$ and $K_L^0$ sideband regions, as indicated in Fig. 1, are investigated. More specifically, the sideband ranges are defined as $10$ MeV/$c^2< |M_{\pi^+\pi^-} - m_{K_S^0}| < 15$ MeV/$c^2$ and $20$ MeV/$c^2 < |M_{p\bar{p}K_S^0}^{\rm rec} - m_{K_L^0}| < 35$ MeV/$c^2$. The sideband events do not form a peaking background around the $\phi$ nominal mass in the $M_{p\bar{p}}^{\rm rec}$ spectrum. In

addition, the other background sources are examined by analyzing the inclusive MC sample of $J/\psi$ decay. The potential background contributions from the inclusive MC sample are found to be the channels with $p\bar{p}\pi^+\pi^-\pi^0\pi^0$ final states, such as $J/\psi \to p\bar{p}f_0' \to p\bar{p}K_S^0K_S^0$, and $J/\psi \to p\omega\bar{\Delta}^- + c.c.$, but none of these backgrounds produce a peak around the $\phi$ nominal mass.

## B.   $J/\psi \to p\bar{p}\phi,\ \phi \to K^+K^-$

For $J/\psi \to p\bar{p}\phi$ with $\phi \to K^+K^-$, the final states are $p\bar{p}K^+K^-$. Since the $p\bar{p}\phi$ mass threshold is close to the $J/\psi$ nominal mass, the available kinematic energy for the kaons is small in this reaction. As a consequence, one of the two charged kaons will have a relatively low momentum and is, thereby, difficult to reconstruct. Therefore, the candidate events are required to have three or four charged tracks. The selection criteria for the charged tracks are same as for the proton (anti-proton) as described in the previous subsection. Two of the charged tracks are required to be identified as proton and anti-proton, while the others are required to be identified as kaons.

A one-constraint (1C) kinematic fit is applied in which the missing mass of the undetected kaon is constrained to its nominal mass. In the case where both kaons have been detected, two 1C kinematic fits are performed with the missing $K^+$ or $K^-$ assumptions, and the one with the smallest chi-square is retained. To suppress backgrounds, the chi-square of 1C kinematic fit is required to be less than 10.

After the above selection criteria, the background contamination is investigated using the inclusive $J/\psi$ MC sample. Besides the irreducible backgrounds from non-resonant $J/\psi \to p\bar{p}K^+K^-$, the reducible background is evaluated to be 20% of all selected events, dominated by the processes involving $\Lambda$ ($\bar{\Lambda}$) intermediate states. To suppress the above backgrounds, all other charged tracks except for the selected proton, antiproton and kaon candidates are assumed to be pions, and the events are vetoed if any combination of $p\pi^-$ or $\bar{p}\pi^+$ has an invariant mass lying in the range $|M_{p\pi^-(\bar{p}\pi^+)} - M_{\Lambda(\bar{\Lambda})}| < 10$ MeV/$c^2$. The $\Lambda$ ($\bar{\Lambda}$) veto requirement retains about 97% of the signal events while rejecting about two-thirds of corresponding reducible backgrounds.

The $K^+K^-$ invariant mass distribution after applying all the above mentioned selection criteria is shown in Fig. 2 (b). A clear $\phi$ peak, corresponding to the signal of $J/\psi \to p\bar{p}\phi$, is observed. Using the inclusive $J/\psi$ MC sample, the main backgrounds are found to be the processes of $J/\psi \to \Lambda(1520)\bar{\Lambda}(1520)$ and $J/\psi \to pK^-\Lambda(1520) + c.c.$ with $\Lambda(1520) \to pK$. These processes can be seen in the data as well, but none of these backgrounds contribute to the $\phi$ peak.
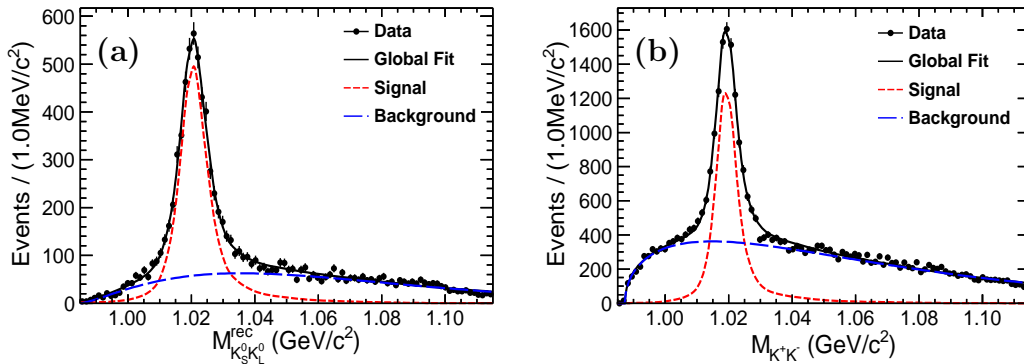
Figure 2. Fits to (a) the recoil mass spectrum against the $p\bar{p}$ system of the $p\bar{p}K_S^0K_L^0$ candidates and (b) the $K^+K^-$ invariant mass spectrum of the $p\bar{p}K^+K^-$ candidates. The black solid lines are the global fit results, the short dashed lines are the signal shapes, and the long dashed lines represent the background shapes.

## IV. MEASUREMENT OF $\mathcal{B}(J/\psi \to p\bar{p}\phi)$

The signal yields of $J/\psi \to p\bar{p}\phi$ for the two decay modes are obtained from unbinned maximum likelihood fits to the $M_{p\bar{p}}^{\rm rec}$ and $M_{K^+K^-}$ mass spectra. In the fit of each mode, the $\phi$ signal is described by the line shape obtained from the MC simulation convoluted with a Gaussian function, which accounts for the difference of mass resolution between the data and the MC. The background shape is parameterized by an ARGUS function [31]. The parameters of the Gaussian function and the ARGUS function are left free in the fit. The projections of the fits are shown in Fig. 2, and the signal yields are listed in Table. I.

The detection efficiencies are obtained by MC simulations that are, in the first instance, based on a PHSP three-body decay of the signal mode $J/\psi \to p\bar{p}\phi$. However, it is found that data deviate strongly from the PHSP MC distributions, as the histograms shown in Fig. 3, where, to subtract the backgrounds, the signal yields of data in each bin are extracted by fitting the $\phi$ signal in the $K\bar{K}$ invariant mass. The detection efficiency varies significantly at low momenta of proton and anti-proton, and, therefore, strongly depends on the $p\bar{p}$ invariant mass. To obtain a more accurate detection efficiency, the events of the PHSP MC are weighted according to the observed $p\bar{p}$ mass distribution, where the weight factor is the ratio of $p\bar{p}$ mass distributions between data and the PHSP MC in Fig. 3 (b) and (f). The average detection efficiencies are determined to be $(30.8 \pm 0.2)\%$ and $(28.9 \pm 0.1)\%$ for $\phi \to K_S^0K_L^0$ and $\phi \to K^+K^-$, respectively. The weighted PHSP MC distributions of the $p\bar{p}$, $p\phi$ and $\bar{p}\phi$ invariant masses are approximately consistent with the background-subtracted data, as shown by the solid lines in Fig. 3. As for the small discrepancies between the weighted PHSP MC and the data, a secondary reweighting is performed based on the present results, and the difference is considered as a systematic uncertainty.

The branching fraction of $J/\psi \to p\bar{p}\phi$ is calculated using

$$\mathcal{B}(J/\psi \to p\bar{p}\phi) = \frac{N_{\rm obs}}{N_{J/\psi} \times \varepsilon \times \mathcal{B}(\phi \to K\bar{K})}, \quad (1)$$

where $N_{\rm obs}$ is the number of signal yields from the fit, $N_{J/\psi} = (1.31 \pm 0.01) \times 10^9$ is the total number of $J/\psi$ events [21] determined from $J/\psi$ inclusive decays, $\varepsilon$ is the weighted detection efficiency obtained as described above, and $B(\phi \to K\bar{K})$ represents the branching fraction of $\phi \to K_S^0K_L^0$ or $\phi \to K^+K^-$, taking into account the branching fraction of $K_S^0 \to \pi^+\pi^-$.

The branching fractions of $J/\psi \to p\bar{p}\phi$ measured using the two $\phi$ decay modes are summarized in Table I. The results are consistent with each other within statistical uncertainties. These two branching fractions are combined using a weighted least-square approach [32], where the systematic uncertainties on the tracking and PID efficiencies of proton and anti-proton as well as the number of $J/\psi$ events are common for the two decay modes, and the remaining systematic uncertainties are independent for each mode. The systematic uncertainties are discussed in detail in the next section. The combined branching fraction, $\mathcal{B}(J/\psi \to p\bar{p}\phi)$, is calculated to be $(5.23 \pm 0.06 \pm 0.33) \times 10^{-5}$, where the first uncertainty is the statistical and the second systematic.

Table I. Signal yields, weighted detection efficiencies and the branching fractions of $J/\psi \to p\bar{p}\phi$ measured by the two decay modes. The first errors are statistical and the second systematic (see Section V).

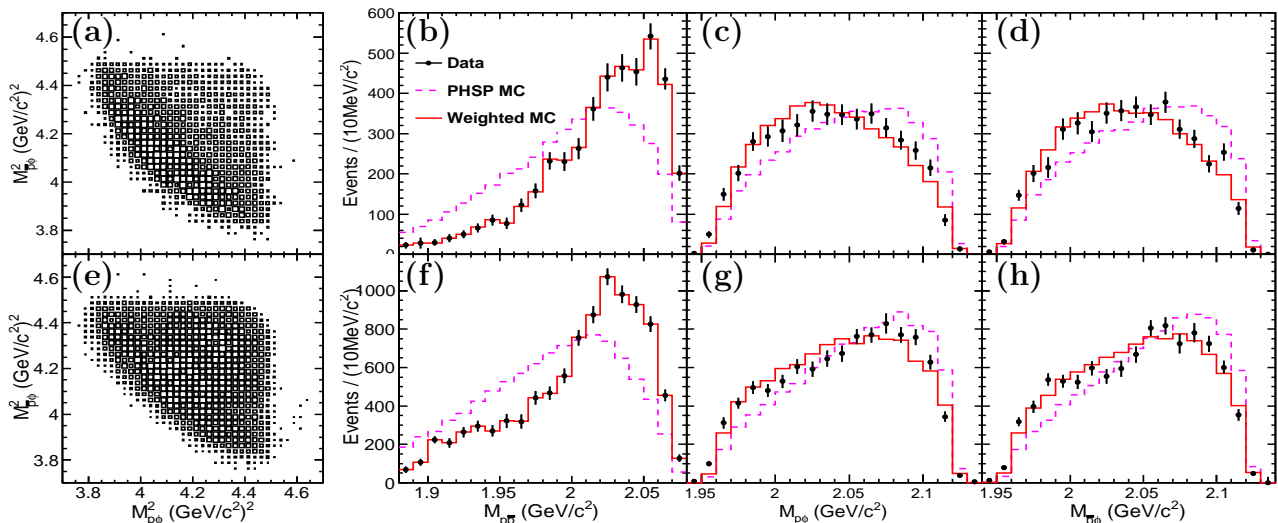| $\phi$ decay mode | $N_{\rm obs}$ | $\varepsilon(\%)$ | $\mathcal{B}(J/\psi \to p\bar{p}\phi)$ |
|---|---|---|---|
| $\phi \to K_S^0K_L^0$ | $4932\pm101$ | $30.8\pm0.2$ | $(5.17\pm0.11\pm0.44)\times10^{-5}$ |
| $\phi \to K^+K^-$ | $9729\pm148$ | $28.9\pm0.1$ | $(5.25\pm0.08\pm0.43)\times10^{-5}$ |

Figure 3. Dalitz plots of the data and the $p\bar{p}$, $p\phi$, and $\bar{p}\phi$ invariant masses. The upper row (a, b, c, d) and the lower row (e, f, g, h) correspond to $\phi \to K_S^0 K_L^0$ and $\phi \to K^+ K^-$, respectively. The dots with error bars represent the background-subtracted data, the dashed histograms represent the PHSP MC simulations, and the solid histograms represent the reweighted MC simulation.

## V. SYSTEMATIC UNCERTAINTIES

The systematic uncertainties are estimated by taking into account the differences in efficiencies between data and MC for the tracking and PID algorithms, the $K_S^0$ reconstruction, the $K_S^0/K_L^0$ mass window requirement, the kinematic fit and the $\Lambda$ ($\bar{\Lambda}$) veto. In addition, the uncertainties associated with the mass spectrum fit, the weighting procedure, as well as the branching fraction of the intermediate state decay and the total number of $J/\psi$ events are taken into consideration.

1) **MDC tracking:** the MDC tracking efficiencies of $p/\bar{p}$ and $K^\pm$ are measured using clean samples of $J/\psi \to p\bar{p}\pi^+\pi^-$ and $J/\psi \to K_S^0 K^\pm \pi^\mp$ [33, 34], respectively. The difference in tracking efficiencies between data and MC is 1.2% for protons, 1.9% for antiprotons, and 1.0% for kaons. The systematic uncertainty associated with the tracking efficiency of $\pi^\pm$ is included in the uncertainty of $K_S^0$ reconstruction.

2) **PID efficiency:** To estimate the PID efficiency uncertainty, we study $p/\bar{p}$ and $K^\pm$ PID efficiencies with the same control samples as those used in the tracking efficiency. The average PID efficiency difference between data and MC is found to be 2% per charged track and taken as a systematic uncertainty.

3) **$K_S^0$ reconstruction:** the $K_S^0$ reconstruction involves the charged-track reconstruction of the $\pi^+\pi^-$ pair and a second vertex fit. The corresponding systematic uncertainty is estimated using a control sample of the decay $J/\psi \to \phi K_S^0 K^\pm \pi^\mp$. The

relative difference in the reconstruction efficiencies of the $K_S^0$ between data and MC is 4.2% and taken as a systematic uncertainty.

4) **$K_S^0$ and $K_L^0$ mass window:** Due to the difference in the mass resolutions between data and MC, the uncertainty related with the $K_S^0$ or $K_L^0$ mass window requirement is investigated by smearing the MC simulation in accordance with the signal shape of data. The changes on the detection efficiencies, 1.3% and 2.5%, are assigned as the systematic uncertainties for the $K_S^0$ and $K_L^0$ mass window requirements, respectively.

5) **1C kinematic fit:** To estimate the systematic uncertainty from the 1C kinematic fit, a clean control sample $J/\psi \to pK^-\bar{\Lambda} + c.c.$ is selected without using a kinematic fit. The efficiency of 1C kinematic fit is estimated by the ratio of signal yields with ($\chi_{1C}^2 < 10$ required) and without 1C kinematic fit. The corresponding difference in the efficiencies between data and MC is found to be 1.4% and taken as a systematic uncertainty.

6) **$\Lambda/\bar{\Lambda}$ veto:** the requirement $|M_{p\pi^-/\bar{p}\pi^+} - M_{\Lambda/\bar{\Lambda}}| > 10$ MeV/$c^2$ is applied to veto $\Lambda/\bar{\Lambda}$ background events. The alternative choices $|M_{p\pi^-/\bar{p}\pi^+} - M_{\Lambda/\bar{\Lambda}}| > 5$ MeV/$c^2$, or $> 15$ MeV/$c^2$ are implemented to recalculate the branching fraction. The maximum difference of the final results, 0.6%, is taken as a systematic uncertainty.

7) **Mass spectrum fit:** The systematic uncertainty associated with the fit of the mass spectrum comes from the parameterization of the signal shape, the background shape and the fit range. To estimate

the uncertainty from the $\phi$ signal shape, we perform an alternative fit with an acceptance corrected Breit-Wigner to describe the $\phi$ signal shape. The uncertainty associated with the smooth shape of the background underneath the $\phi$ peak is evaluated by replacing the ARGUS function with a function of $f(M) = (M - M_a)^c (M_b - M)^d$, where, $M_a$ and $M_b$ are the lower and upper edges of the mass distribution, respectively; $c$ and $d$ are free parameters. The uncertainty due to the fit range is estimated by fitting within the alternative ranges. The change of signal yield in the different fit scenarios is taken as the corresponding systematic uncertainty. The quadratic sums of the three individual uncertainties, 3.9% and 1.9%, for $\phi \to K_S^0 K_L^0$ and $\phi \to K^+ K^-$, respectively, are taken as the systematic uncertainty related with the mass spectrum fit.

8) **Weighting procedure:** To obtain a reliable detection efficiency, the PHSP MC sample is weighted to match the distribution of the background-subtracted data. To consider the effect on the statistical fluctuations of the signal yield in the data, a set of toy-MC samples, which are produced by sampling the signal yield and its statistical uncertainty of the data in each bin, are used to estimate the detection efficiencies. Consider the systematic uncertainty on the secondary reweighting, the resulting deviations of detection efficiencies, 2.4% and 2.9% for $\phi \to K_S^0 K_L^0$ and $\phi \to K^+ K^-$, respectively, are taken as the systematic uncertainty associated with the weighting procedure.

The contributions of the systematic uncertainties from the above sources and the systematic uncertainties of the branching fractions of intermediate decays ($\phi \to K^+ K^-$ and $K_S^0 \to \pi^+ \pi^-$) as well as the number of $J/\psi$ events [20, 21] are summarized in Table II. The total systematic uncertainties are given by the quadratic sum of the individual uncertainties, assuming all sources to be independent.

## VI. UPPER LIMIT OF $p\bar{p}$ MASS THRESHOLD ENHANCEMENT

The Dalitz plots of the data and the corresponding one-dimensional mass projections presented in Fig. 3 show no significant signatures of a threshold enhancement in the $p\bar{p}$ invariant mass nor obvious structures in the $p\phi$ ($\bar{p}\phi$) mass spectra. The most rigorous procedure is to carry out a PWA. However, due to the small phase space for the decay $J/\psi \to p\bar{p}\phi$ and the lack of a proper physics model, such an analysis is difficult to pursue. In this analysis, we only consider an upper limit for the $p\bar{p}$ mass threshold enhancement by fitting solely the $p\bar{p}$ mass spectrum near the threshold.

To obtain the best upper limit on the $X(p\bar{p})$ yield, the two decay modes are combined to determine the upper limit on the branching fraction of $J/\psi \to X(p\bar{p})\phi \to p\bar{p}\phi$. A least squares simultaneous fit is performed on both $p\bar{p}$ invariant mass distributions of the two $\phi$ decay modes around the mass threshold. The two decay modes share the same branching fraction

$$\mathcal{B} = \frac{N_{\text{obs}}}{N_{J/\psi} \cdot \mathcal{B}(\phi \to K\bar{K}) \cdot \varepsilon \cdot (1 - \sigma_{\text{sys}})}, \qquad (2)$$

where $N_{\text{obs}}$ represents the $X(p\bar{p})$ signal yield of each decay mode corresponding to the given test $\mathcal{B}(J/\psi \to X(p\bar{p})\phi \to p\bar{p}\phi)$, $N_{J/\psi}$ and $\mathcal{B}(\phi \to K\bar{K})$ are same as described in Eq. 1, $\varepsilon$ is the detection efficiency of $X(p\bar{p})$ obtained from MC simulations (14.4% for the mode $\phi \to K_S^0 K_L^0$, while 21.4% for $\phi \to K^+ K^-$), $\sigma_{\text{sys}}$ is the total relative systematic uncertainty as reported in Table II. With such a method, a combined upper limit on the branching fraction, $\mathcal{B}^{\text{UL}}$, at a 90% C.L. can be determined directly.

In the simultaneous fit, the spin and parity of $X(p\bar{p})$ are set to be $0^{-+}$ based on earlier BESIII observations [4], and effects of interference are neglected. The signal of $X(p\bar{p})$ is parameterized by an acceptance-weighted $\mathcal{S}$-wave Breit-Wigner function

$$BW(M) \simeq \frac{f_{\text{FSI}} \times q^{2L+1} \kappa^3}{(M^2 - M_0^2)^2 + M_0^2 \Gamma_0^2} \times \varepsilon_{\text{rec}}(M), \qquad (3)$$

where $M$ is the $p\bar{p}$ invariant mass, $q$ is the momentum of the proton in the $p\bar{p}$ rest frame, $\kappa$ is the momentum of the $\phi$ in the $J/\psi$ rest frame, $L = 0$ is the relative orbital angular-momentum of $p\bar{p}$ system, $M_0$ and $\Gamma_0$ are the mass and width of the $X(p\bar{p})$ [4], $\varepsilon_{\text{rec}}(M)$ is the detection efficiency as a function of $p\bar{p}$ invariant mass, which is obtained from the MC simulations of $J/\psi \to X(p\bar{p})\phi \to p\bar{p}\phi$ by taking into account the helicity angular distributions, the parameter $f_{\text{FSI}}$ accounts for the effect of the FSI.

To take into account the systematic uncertainties related to the fit procedure of the $X(p\bar{p})$, three aspects with different fit scenarios are considered: (1) excluding the FSI factor (corresponding to $f_{\text{FSI}}=1$); taking into account the Jülich FSI value for FSI [14]; (2) the non-resonant backgrounds both parameterized by a function of $f(\delta) = N(\delta^{1/2} + a_1 \delta^{3/2} + a_2 \delta^{5/2})$ ($\delta = M_{p\bar{p}} - 2m_p$, $m_p$ is the proton mass, $a_1$ and $a_2$ are free parameters); or both represented by the shape obtained from the $J/\psi \to p\bar{p}\phi$ MC simulation; (3) the fit ranges both in [0.0, 0.140] or in [0.0, 0.150] GeV/$c^2$. By combining these three different aspects, we perform in total eight alternative fit scenarios. The fit scenario taking into account the FSI, with the non-resonant backgrounds parameterized by the function, and the fit ranges both in [0.0, 0.140] GeV/$c^2$, gives the maximum upper limit on the branching fraction, which is shown in Fig. 4, where the efficiency as a function of the $p\bar{p}$ mass is also plotted. The combined upper limit at the 90% C.L. is determined to be $2.1 \times 10^{-7}$.

Table II. Summary of the systematic uncertainties in the branching fraction measurement (in %), the items with ... denote that the corresponding systematic uncertainty is not applicable.

| Sources | $\phi \to K_S^0 K_L^0$ | | $\phi \to K^+ K^-$ | |
|---|---|---|---|---|
| | $\mathcal{B}(J/\psi \to p\bar{p}\phi)$ | $\mathcal{B}(J/\psi \to X(p\bar{p})\phi \to p\bar{p}\phi)$ | $\mathcal{B}(J/\psi \to p\bar{p}\phi)$ | $\mathcal{B}(J/\psi \to X(p\bar{p})\phi \to p\bar{p}\phi)$ |
| MDC tracking | 3.1 | 3.1 | 4.1 | 4.1 |
| PID efficiency | 4.0 | 4.0 | 6.0 | 6.0 |
| $K_S^0$ reconstruction | 4.2 | 4.2 | ... | ... |
| $K_S^0$ mass window | 1.3 | 1.3 | ... | ... |
| $K_L^0$ mass window | 2.5 | 2.5 | ... | ... |
| 1C kinematic fit | ... | ... | 1.4 | 1.4 |
| $\Lambda(\bar{\Lambda})$ veto | ... | ... | 0.6 | 0.6 |
| Mass spectrum fit | 3.9 | ... | 1.9 | ... |
| Weighting procedure | 2.4 | ... | 2.9 | ... |
| Number of $J/\psi$ events | 0.8 | 0.8 | 0.8 | 0.8 |
| $\mathcal{B}(\phi \to K\bar{K})$ | 1.2 | 1.2 | 1.0 | 1.0 |
| $\mathcal{B}(K_S^0 \to \pi^+\pi^-)$ | 0.1 | 0.1 | ... | ... |
| Total | 8.6 | 7.3 | 8.3 | 7.5 |
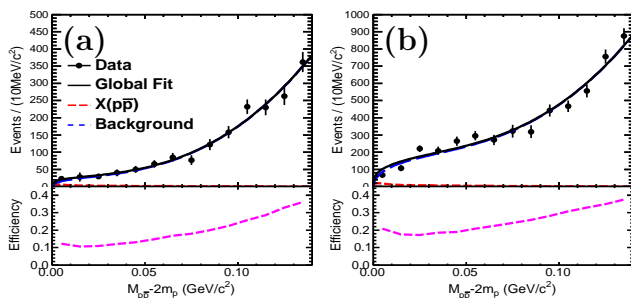


Figure 4. Distributions of $M_{p\bar{p}} - 2m_p$ and the fit results corresponding to the upper limit on the branching fraction at the 90% C.L., the dashed line at the bottom is the efficiency as a function of the $p\bar{p}$ mass, (a) for $\phi \to K_S^0 K_L^0$, (b) for $\phi \to K^+ K^-$.

## VII. SUMMARY

Based on a sample of $1.31\times10^9$ $J/\psi$ events accumulated at BESIII, we present a study of $J/\psi \to p\bar{p}\phi$ with two decay modes $\phi \to K_S^0 K_L^0$ and $\phi \to K^+ K^-$. The branching fraction of $J/\psi \to p\bar{p}\phi$ is measured to be $[5.23 \pm 0.06\,(\text{stat}) \pm 0.33\,(\text{syst})] \times 10^{-5}$, which is consistent with the previous measurement [19], but with a significantly improved precision. We have neither observed a significant structure in the $p\phi$ or $\bar{p}\phi$ mass spectra, nor found evidence of an enhancement in the $p\bar{p}$ mass spectrum near its threshold. The corresponding upper limit on the branching fraction of $J/\psi \to X(p\bar{p})\phi \to p\bar{p}\phi$ is determined to be $2.1 \times 10^{-7}$ at a 90% C.L.. With the production branching fraction of $J/\psi \to \gamma X(p\bar{p}) \to \gamma p\bar{p}$, $[9.0^{+0.4}_{-1.1}\,(\text{stat})^{+1.5}_{-5.0}\,(\text{syst}) \pm 2.3\,(\text{model})] \times 10^{-5}$ [4], the upper limit on the decay rate ratio of $\mathcal{B}(J/\psi \to X(p\bar{p})\phi)/\mathcal{B}(J/\psi \to \gamma X(p\bar{p}))$ is calculated to be $[0.23^{+0.01}_{-0.03}\,(\text{stat})^{+0.04}_{-0.13}\,(\text{syst}) \pm 0.06\,(\text{model})]\%$.

Though no clear structure in the $p\bar{p}$, $p\phi$ and $\bar{p}\phi$ mass spectra is observed in this analysis, the data appear to significantly deviate from a naive PHSP distribution.

This implies the existence of interesting dynamical effects, such as intermediate resonances. With the presented analysis, it is difficult to study them in detail due to the small phase space of the decay $J/\psi \to p\bar{p}\phi$. The study of analogous decay processes with larger phase space, such as $\psi(3686) \to p\bar{p}\phi$, in combination with a PWA, may shed light and help to understand their dynamical origins.

## VIII. ACKNOWLEDGMENTS

[1] J. Z. Bai *et al.* (BES Collaboration), Phys. Rev. Lett. **91**, 022001 (2003).

[2] J. P. Alexander *et al.* (CLEO Collaboration), Phys. Rev. D **82**, 092002 (2010).

[3] M. Ablikim *et al.* (BESIII Collaboration), Chin. Phys. C **34**, 421 (2010).

[4] M. Ablikim *et al.* (BESIII Collaboration), Phys. Rev. Lett. **108**, 112003 (2012).

[5] S. B. Athar *et al.* (CLEO Collaboration), Phys. Rev. D **73**, 032001 (2006).

[6] M. Ablikim *et al.* (BESIII Collaboration), Phys. Rev. Lett. **110**, 022001 (2013).

[7] M. Ablikim *et al.* (BES Collaboration), Eur. Phys. J. C **53**, 15 (2007).

[8] M. Ablikim *et al.* (BESIII Collaboration), Phys. Rev. D **87**, 112004 (2013).

[9] A. Datta and P. J. O'Donnel, Phys. Lett. B **567**, 273 (2003).

[10] M. L. Yan, S. Li, B. Wu, and B. Q. Ma, Phys. Rev. D **72**, 034027 (2005).

[11] S. L. Zhu, Int. J. Mod. Phys. A **20**, 1548 (2005).

[12] M. Abud, F. Buccella, and F. Tramontano, Phys. Rev. D **81**, 074018 (2010).

[13] B. S. Zou and H.C. Chiang, Phys. Rev. D **69**, 034004 (2004).

[14] A. Sibirtsev, J. Haidenbauer, S. Krewald, Ulf-G. Meissner, and A. W. Thomas, Phys. Rev. D **71**, 054010 (2005).

[15] X. W. Kang, J. Haidenbauer and Ulf-G. Meissner, Phys. Rev. D **91**, 074003 (2015).

[16] G. Y. Chen, H. R. Dong, and J. P. Ma, Phys. Lett. B **692**, 136 (2010).

[17] M. Ablikim *et al.* (BES Collaboration), Phys. Rev. Lett. **95**, 262001 (2005).

[18] M. Ablikim *et al.* (BESIII Collaboration), Phys. Rev. Lett. **106**, 072002 (2011).

[19] A. Falvard *et al.* (DM2 Collaboration), Phys. Rev. D **38**, 2706 (1988).

[20] M. Ablikim *et al.* (BESIII Collaboration), Chin. Phys. C **36**, 915 (2012).

[21] With the same approach as for $J/\psi$ events taken in 2009 (see Ref. [20] for more details), the preliminary number of $J/\psi$ events taken in 2009 and 2012 is determined to be $1310.6 \times 10^6$ with an uncertainty of 0.8%.

[22] M. Ablikim *et al.* (BESIII Collaboration), Nucl. Instrum. Meth. A **614**, 345 (2010).

[23] D. M. Asner *et al.*, Int. J. Mod. Phys. A **24**, 499 (2009).

[24] S. Agostinelli *et al.* (GEANT4 Collaboration), Nucl. Instrum. Meth. A **506**, 250 (2003)

[25] Z. Y. Deng *et al.*, HEP & NP **30**, 371 (2006).

[26] S. Jadach, B. F. L. Ward, and Z. Was, Comp. Phys. Commu. **130**, 260 (2000).

[27] S. Jadach, B. F. L. Ward, and Z. Was, Phys. Rev. D **63**, 113009 (2001).

[28] D. J. Lange, Nucl. Instrum. Meth. A **462**, 152 (2001); R. G. Ping, Chin. Phys. C **32**, 599 (2008).

[29] K. A. Olive *et al.* (Particle Data Group), Chin. Phys. C **38**, 090001 (2014).

[30] J. C. Chen, G. S. Huang, X. R. Qi, D. H. Zhang, and Y. S. Zhu, Phys. Rev. D **62**, 034003 (2000).

[31] H. Albrecht *et al.*, Phys. Lett. B **340**, 217 (1994).

[32] G. D'Agostini, Nucl. Instrum. Meth. A **346**, 306 (1994).

[33] M. Ablikim *et al.* (BESIII Collaboration), Phys. Rev. D **83**, 112005 (2011).

[34] M. Ablikim *et al.* (BESIII Collaboration), Phys. Rev. D **85**, 092012 (2012).